

Miocene Polyphase Structural Evolution of the 'I' Field, NW Malay Basin

*Siti Sorhana Syazwani Mokhtar **, *Mohamed Elsaadany*, *Benjamin Sautter* and *Nur Huda M Jamin*

Department of Geoscience, Universiti Teknologi PETRONAS, 32610 Seri Iskandar, Malaysia

Received January 27, 2021; Accepted May 10, 2021

Abstract

The Malay Basin is a structural anomaly characterized by immensely thick Cenozoic sequences located in the relatively stable centre of Sundaland. The Malay Basin's earliest rift started in the Paleogene triggered by an episode of transtension along NW-SE trending shear zone which referred to as the Axial Malay Fault Zone. During the Middle Miocene, a major inversion occurred, causing the reactivation of the Malay Basin axial shear zone and the development of large scale folds. This regional N-S compression originated from the south, likely related to the indentation of Australian Plate in the southern margin of Sundaland. In this study, we focus on the Late Miocene structural evolution of the north-western part of the Malay Basin by computing seismic attribute map and complex seismic trace analysis method such as cosine of phase, variance and chaos attributes derived from post-stack seismic data. Through the interpretation of volume attribute, 3D time-slice, and surface attribute, here we show a network of normal faults active in the Late Miocene to Pliocene-recent which are seen cross-cutting the top of a Middle Miocene anticline and appear to influence the post-Middle Miocene sedimentation. One set of fault striking N-S is crosscut by another set of E-W faults. Based on detailed seismic interpretation and seismic to well tie the E-W faults were active from the Middle Miocene to Lower Pliocene, and the N-S faults between Middle Miocene to Upper Pliocene. The faults post-date the anticline and suggest a minor tectonic episode or sedimentary load driven extension on top of different post inversion morphologies.

Keywords: *Structural evolution; Faulted anticline; Seismic attribute; Basin inversion; Miocene age.*

1. Introduction

The Malay Basin, located at the center of Sundaland (Figure 1), the Cratonic core of South-east Asia, is one of the deepest continental extensional basins in the region and is believed to have formed during early Tertiary times [1]. The Tenggol Arch separates the Malay Basin from Penyu Basin, while Narathiwat High separates the Malay Basin from Thailand's Pattani Basin. The Malay Basin is an elongate NW-SE trending basin, about 500 km long and 250 km wide, underlain by pre-tertiary basement consist of three type of lithogy which are metamorphic, igneous, and sedimentary rocks [1].

The Tertiary tectonic evolution of the Malay Basin has been widely accepted to comprise three main phases. The three main phases are crustal rifting, followed by basin subsidence (thermal subsidence), and compression (structural inversion) [2]. Meanwhile, [3] has classified the Malay basin into 5 phases: the pre-rift phase, the syn-rift phase, the fast subsidence phase, the compression phase, and the basin sag phase. From the Middle Miocene onward the basin is considered to be relative tectonic quiescence by most authors (Mansor, Hall, Tjia and Yazid). However, from this study we can see a few faults can still be active due to sediment load or from any tectonic movement.

During the Middle-Late Miocene, the Malay Basin has undergone inversion, which resulted in developing a large wrench-induced compressional anticline, mostly within the basin's axial region [1] and [4]. Tjia has described the structural evidence of basin inversion, which are compressional anticlines, inverted, uplifted half-graben, and reverses throws on normal faults [5].

The inversion anticline's geometry and location come out to have been strongly controlled by the basement faults in Neogene sedimentary till along the Axial Malay Fault Zone (AMFZ), which were produced by the sinistral slip of the Axial Malay Fault Zone during basin inception. The inversion anticlines then formed over the half-graben by an NW trending dextral shear during the basin inversion phase. The southeastern part of the basin's structure is typified by tightly folded post-rift strata that once filled the half-graben. The bounding faults to the half-graben have been reactivated as reverse and/or strike-slip faults. The structures have complex upward diverging geometries and typical of positive flower structures associated with wrench faulting. The flower structures may have formed by sinistral oblique-slip reactivation of their East trending half-graben border faults due to the reversal in the shear direction [1].

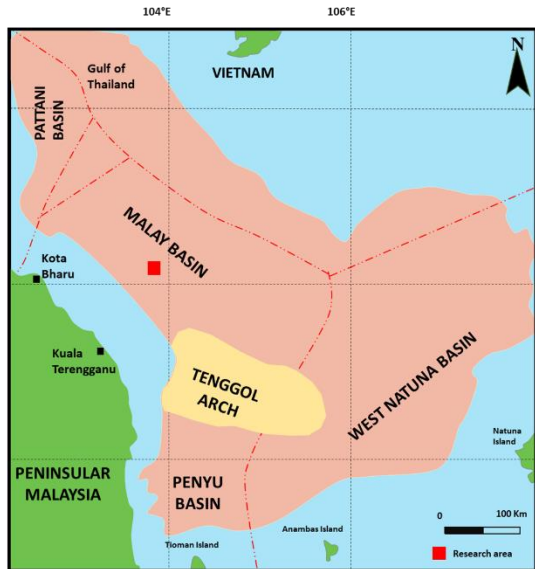


Figure 1. Show the research area that located in Northern Malay Basin, modified after [1,6]

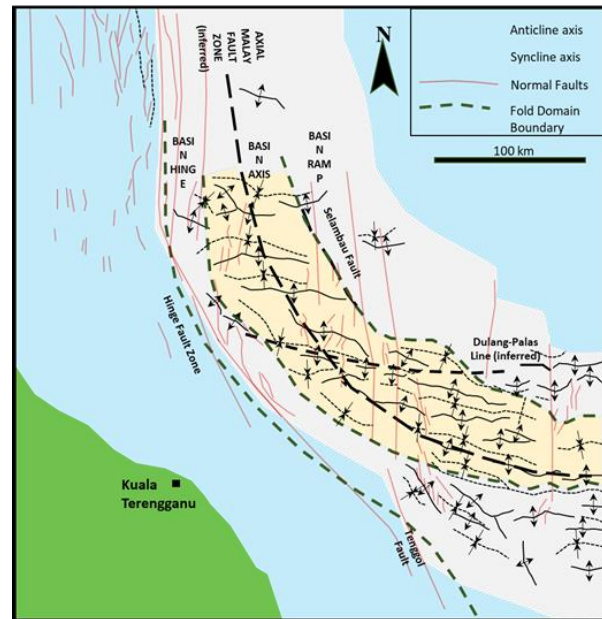


Figure 2. Show the major structural features and fold domain of the Malay Basin (grey-shaded area), modified after [2,4]

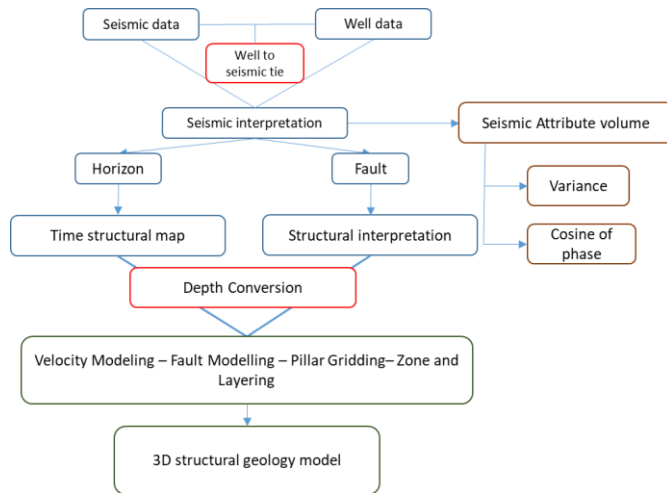
In this paper we demonstrate fault reactivation in the Late Miocene to Pliocene, by making use of high resolution 3D seismic data and well logs. The cover study area approximately of 3305.97 km² and it consists of several big gas discoveries with moderate to high CO₂ contents ranges from 4 to 75%. The well discovered gas in stacked reservoirs of Group B, D and E sands and minor oil in the Group E (Figure 3).

Geological Age	Group	Fault Block	North West		South West		East				
		Well Name	Well-4	Well-5	Well-3	Well-Deep 1	Well-1	Well-2	Well-6	Well-7	Well-8
		Well Profile	Vertical Oil and Gas show	Vertical Oil and Gas show	Vertical Gas show	Vertical Gas show	Vertical Oil and Gas discovery	Vertical Gas discovery	Vertical Gas show	Vertical Oil and Gas show	Vertical Gas show
Pleistocene-Recent	A								877		
Pliocene	Upper										
	Lower		1227.73	1190.55	1241.45	1200	1163.42	1196.34	1276	1298	1316.39
Miocene	Upper	D	1522.17	1477.67	1628.55	1506	1551.43	1597.15	1425	1533	1610.20
		E	TD at 1806.85	TD at 1107.42	TD at 1883.96	1913	TD at 1803.36	TD at 1803.75	TD at 1557	TD at 2042	2212.89
	Middle	F				2387					TD at 2266.99
		H				TD at 2056					

Figure 3. Show the well penetrated of study area with present of gas and oil

Our computed attribute map shows clear offsets of the inversion structure which are folding anticline occurred during basin compression and some faults (Figure 4 and 5). This study area structure is an east-west trending anticline intersected by numerous north-south normal faults and an east-west trending fault (Figure 7). Finally, we propose a 3D structural model to illustrate the tectonic evolution of the region during and after the basin inversion which happened in Miocene Age.

2. Materials and methods



We incorporated this seismic cube data into a commercial interactive 3D visualization, analysis, and modeling program using Petrel 2018 and integrated with the well data in 2D interpretation on individual seismic lines for later 3D mapping.

Figure 2. Workflow for seismic interpretation

2.1. Structural attribute for fault interpretation

The best location of the faults system was identified by looking at the 3D seismic cube and applying seismic attribute volume in the time slice section. The 3D time slice works by analyzing differences in seismic wave amplitude. The most reliable fold and fault systems were identified at -1400 ms. Seismic section inline and crossline were interpreted for fault and horizon picking to produce a structural map. In Figures 4 and 5, two volumes attribute which are variance combined with chaos and cosine of phase have been applied to enhance the appearance and quality of the seismic data for fault identification. The seismic data cube was integrated with well data.

These attributes helped to improve 3D seismic data quality and resolution with respective parameters [4]. For structural studies, seismic attributes mapping became most important to identify large structures, but it also can be used to determine sub-seismic fault offsets of less than 10-20 m.

The selection of stratigraphy reference horizons was determined based on the reflective character, lateral continuity, and focused on group D and E which are prone gas reservoir in this field. Various interpreted reference horizons were exported to create a surface map using Petrel. The data computation of strike, dip direction and dip angle was conducted on Paleoscan software to create georse diagram and stratigraphic projection diagrams (stereonet).

Fault system in the 2D map view was studied by using multi-attribute (Variance and chaos) and single volume attribute (cosine of phase) applied by time slice in the two-way time domain at -1400 ms. As we can see in figure 4, Variance and chaos attribute were combined to get the better image of faults in time slice map and the cosine of phase we can see the termination of faults in the seismic section of inline 3161 (Figure 5). This attribute clearly show the horizon terminated by faults which helping for determine the age of the faults.

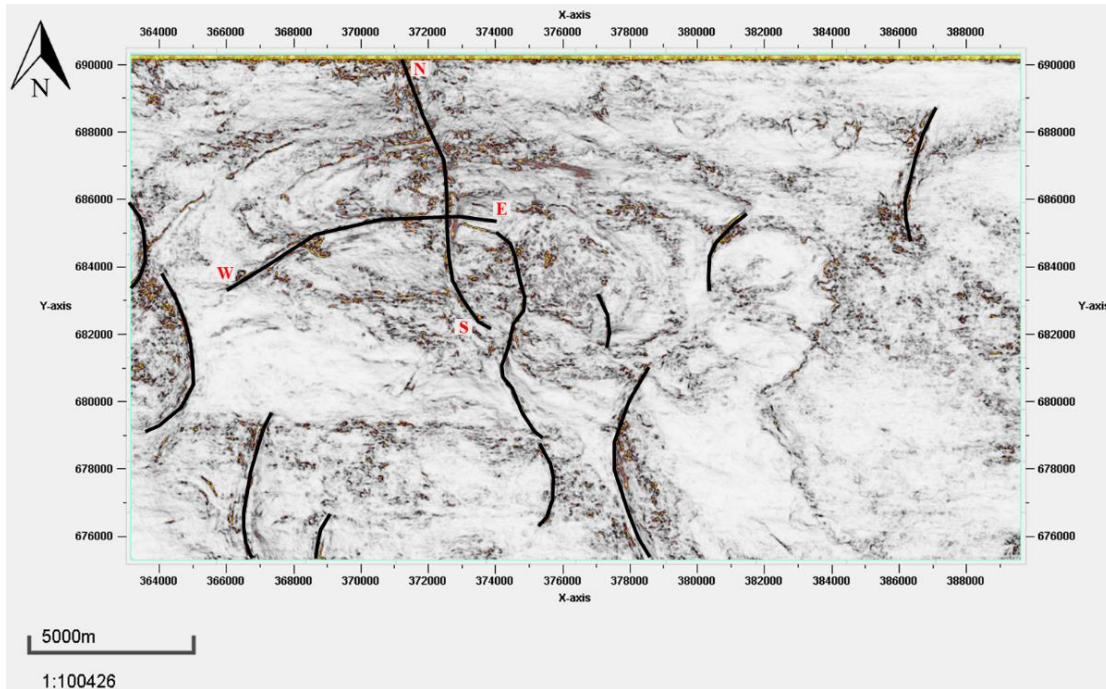


Figure 4. Multi-attribute (variance attribute blending with chaos attribute) map in time domain that show the set of faults lineament (in the red circle).

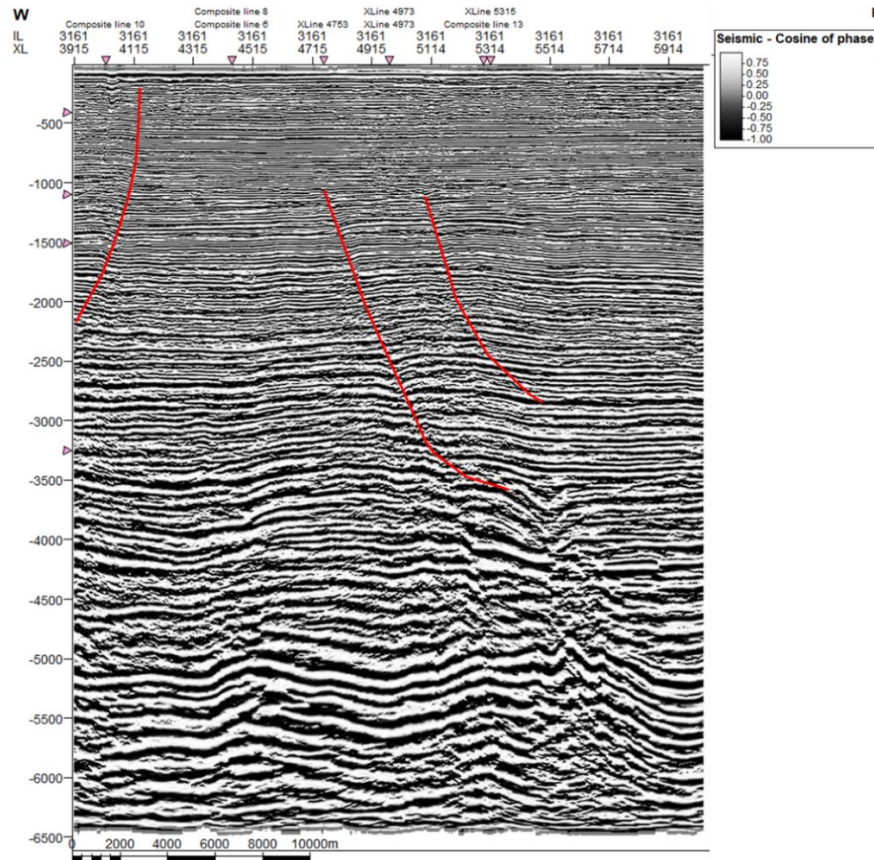


Figure 5. Cosine of phase attribute in seismic section inline 3161 that showed the fault termination

3. Results and discussion

3.1. Structural interpretation

The fault interpretation was started by picking fault segment in both seismic section inline and crossline in 2D view. A total of 13 normal faults was labelled as F1 to F13 and delineated in the seismic section, Figure 6. The length of the fault planes ranges from 0.5 to 3 km. Most of the faults strike north-south direction with dips toward the east with only three faults dipping west and 1 major faults strikes east-west with dip towards the north. The dip direction, dip angle and strike of the mapped faults were simplified in Table 2. Two major faults (one N-S and one E-W) crosscut the anticline revealing that fault activity post -dates basin inversion, Figure 7. The local stress field is characterized by a consistent E-W extension as illustrated by the stratigraphic projection (stereonet), Figure 8.

Table 1. Reading of strike, dip direction and dip angle.

Fault name	Strike	Dip Direction	Dip Angle	Lmax (m)	Height (m)	Dmax (m)	Class	Type	Age	
F1	4	East	94°	33°	4435.46	5016.76	126.29	Long	Normal	Early Miocene- Upper Pliocene
F2	9	East	99°	38°	1156.33	2622.54	78.66	Medium	Normal	Late Miocene- Pleistocene
F3	354	East	84°	30°	5829.74	8212.26	111.95	Long	Normal	Early Miocene-Pleistocene
F4	177	West	267°	33°	3263.25	4872.41	120.93	Long	Normal	Middle Miocene-Lower Pliocene
F5	185	West	275°	32°	6773.45	2775.54	128.17	Long	Normal	Late Miocene-Lower Pliocene
F6	351	East	81°	26°	7631.76	4458.39	191.8	Long	Normal	Middle Miocene-Late Miocene
F7	351	East	81°	31°	9422.4	6321.74	321.4	Long	Normal	Early Miocene-Upper Pliocene
F8	172	West	262°	36°	1689.96	1176.13	78.7	Medium	Normal	Late Miocene-Lower Pliocene
F9	189	West	279°	40°	4257.66	1510.3	6.01	Long	Normal	Lower Pliocene-Pleistocene
F10	27	East	117°	35°	3800.92	3752.93	0	Long	Normal	Middle Miocene-Late Miocene
F11	30	East	120°	31°	2312.05	1025.66	97.38	Medium	Normal	Late Miocene-Lower Pliocene
F12	13	East	103°	36°	4675.23	4093.41	104.74	Long	Normal	Middle Miocene-Late Miocene
F13	254	South	344°	37°	10013.98	2507.52	120.07	Long	Normal	Early Miocene-Lower Pliocene

This network of normal faults was active in the late Miocene to Pliocene-recent which determine by fault plane that is crosscut the top of the anticline. Based on cross-cutting relationship, the E-W fault (F13) was active between the Middle Miocene to Lower Pliocene and the N-S faults were active between Middle Miocene to Upper Pliocene. The fold structure in this study area appear as a compressional anticline trending WNW-ESE with intersected by numerous N-S major normal faults and one E-W trending major normal fault (F13). This compressional anticline is believed to be controlled by basement faults during basin inversion. In the area, axial basin region, the development of large wrench instigated compressional anticline as a result of basin inversion [8].

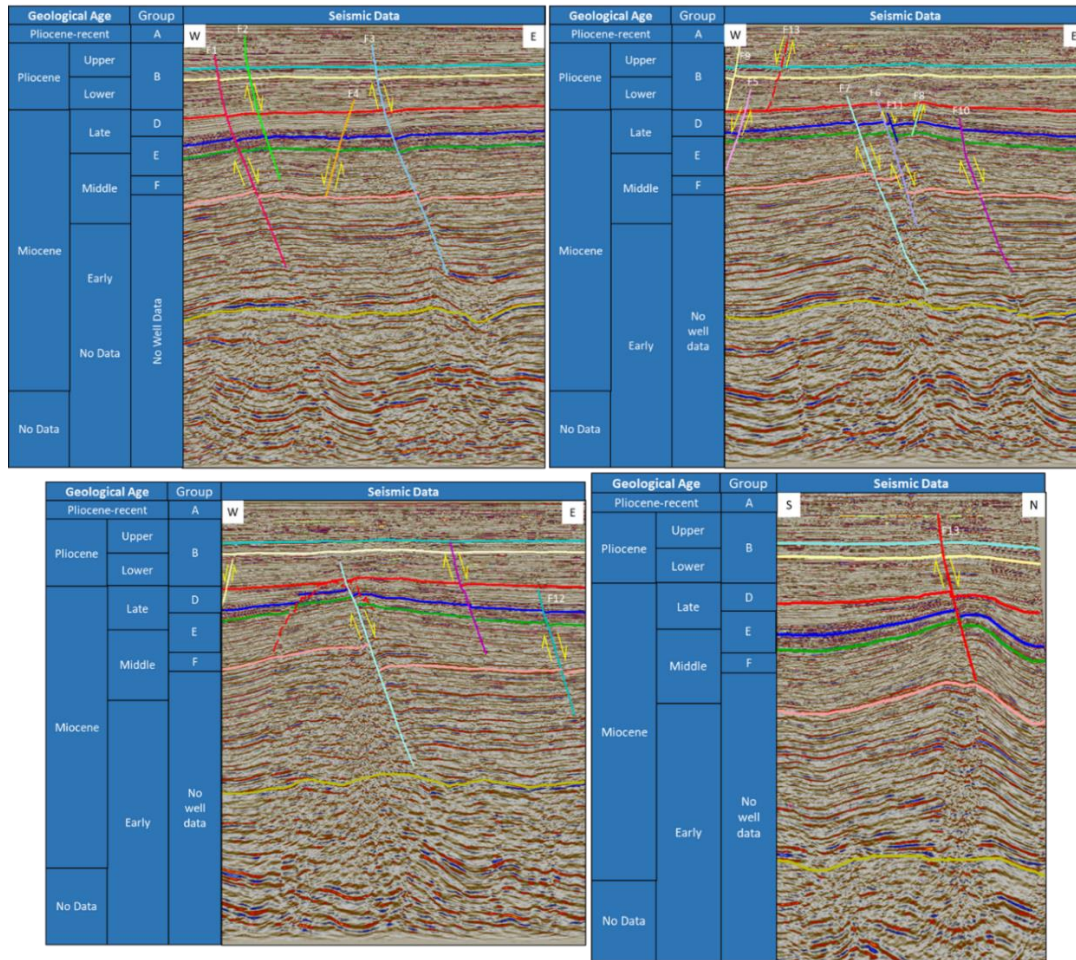


Figure 6. All the faults are labelled as F1 to F13 along the along the 17km E-W line. The color line indicates the position of the time slice cutting through the faults

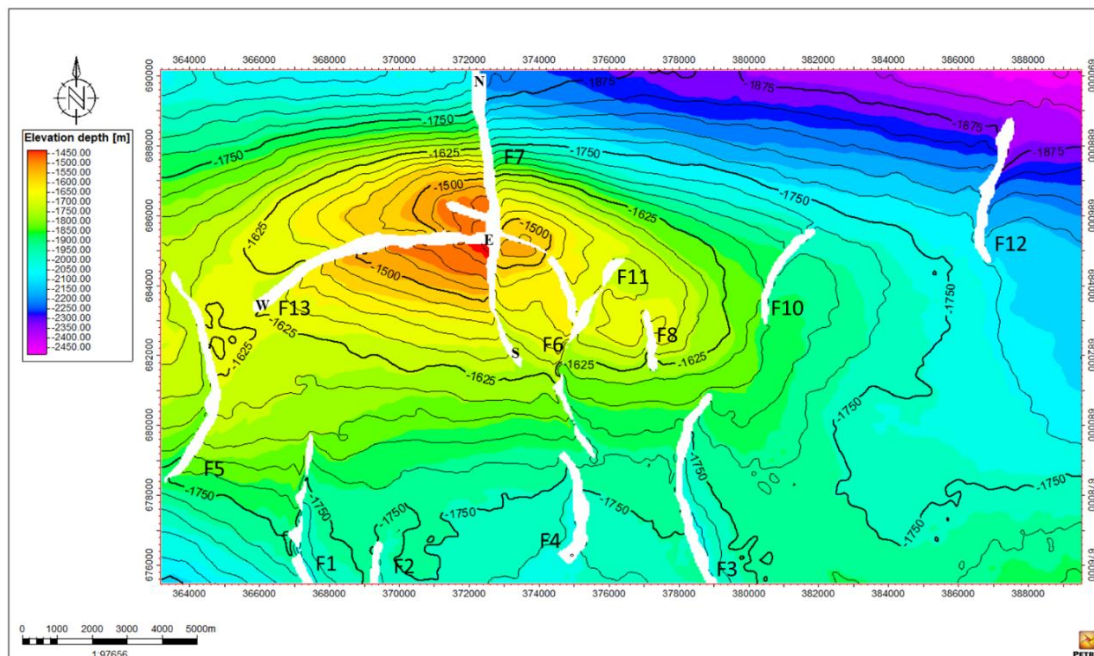


Figure 7. Structural map of the region. A major N-S fault (F7) and E-W fault (F14) cut through the anticline.

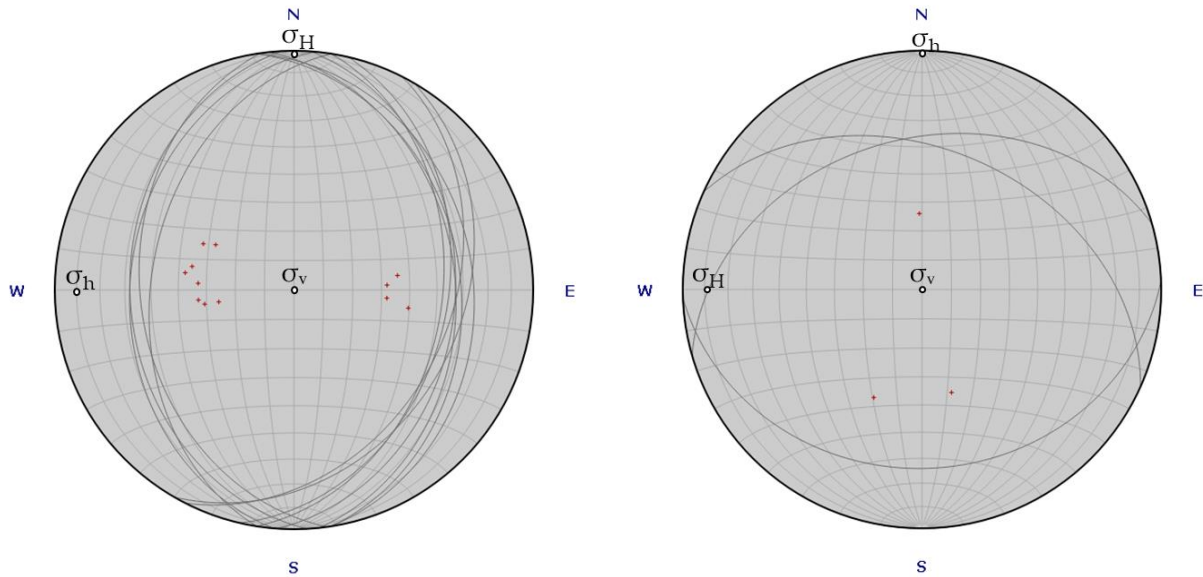


Figure 8. Stratigraphic projection (Stereonet) showing the stress field of the region. The maximum stress is from σ_v and the minimum stress was coming from σ_h

3.2. Miocene polyphase structural evolution

The first phase, Figure 9 (A) shows the illustration model of the evolution of extensional basin and underwent basin inversion based on the interpretation of structural in the study area. In [9], the authors proposed a tectonic origin model of Malay Basin which explained the development of a large extensional basin along a reactivated NW-SE strike-slip zone. Meanwhile, other studies [10] revealed with large shear generating W-E trending faults that originated from India-Asia in early Tertiary. Following both studies, and our structural interpretation in the study area, here we propose a new conceptual model for the tectonic development of the I field NW Malay Basin.

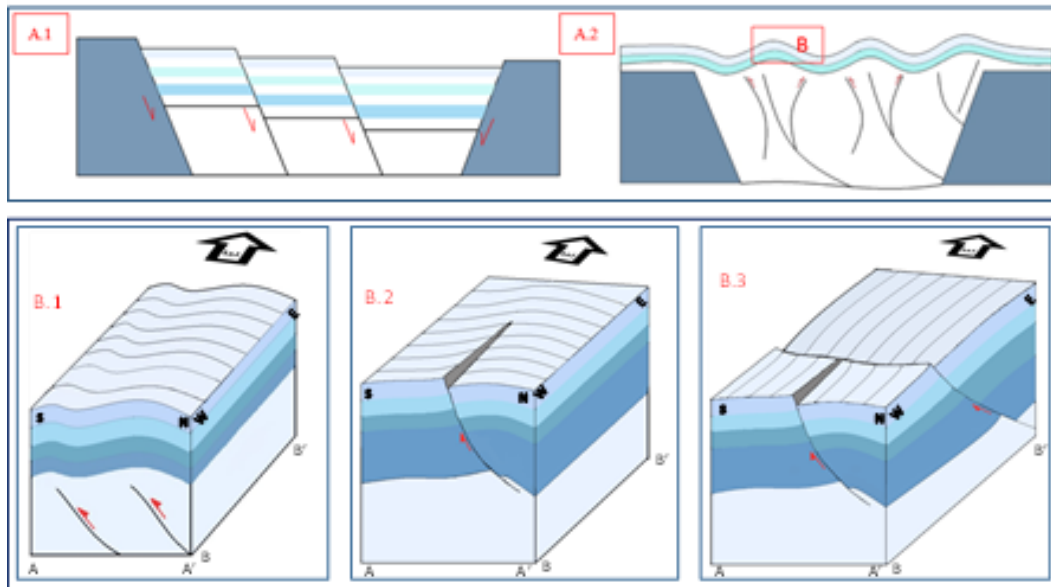


Figure 9. 3D model of structural evolution in I Field. a.1) sketch showing of the initial extension off-stage in the Malay basin, a.2) basin inversion and w-e trending compressional anticlines, b.1) 3D block diagram of the compression controlled by basement fault, b.2) Initiation of the extension along a North-South, b.3) Second stage of the extension along an E-W normal fault that crosscuts the N-S fault and postdate the compressional anticline.

During the Middle to Late Miocene, beginning of basin took place in Malay Basin and a series of E-W trending anticlines and syncline developed during this time (Figure 9 [A.2]) and (Figure 9 [B.1]). According to [11] the fold developed because of a regional shortening across the Sunda Block originating from collision of Indo-Australian plate Oblique with the southern margin of Sunda block and South East Asia. There have two major faults have occurred as shown in model (Figure 9 [B.2] and [B.3]) which the fault E-W and N-S causes the ductile deformation and continues until lower Pliocene (Fault E-W) and upper Pliocene-recent (Fault N-S). Based on primary interpretation on the seismic cube in time slice and seismic cross-section, at the bottom of the seismic line (Figure 10) we observe multiple structures have of folded layers and wavy bedding was interpreted as the result of basin inversion (compression) during the Middle Miocene. Moreover, along the blue fault the bottom segment highlighted in the red circle evidence a reverse offset whereas the top segment shows a normal offset (yellow circle). This fault is interpreted as being active by the end of the compression event in the Early to Middle Miocene and later reactivated during the extension in the Middle Miocene to Pliocene. Figure 10 indicates that the four faults in the seismic section are the result of reactivated faults that caused by sedimentation loading where the fault does not interfere with sedimentation at the age of the late Miocene until to the bottom.

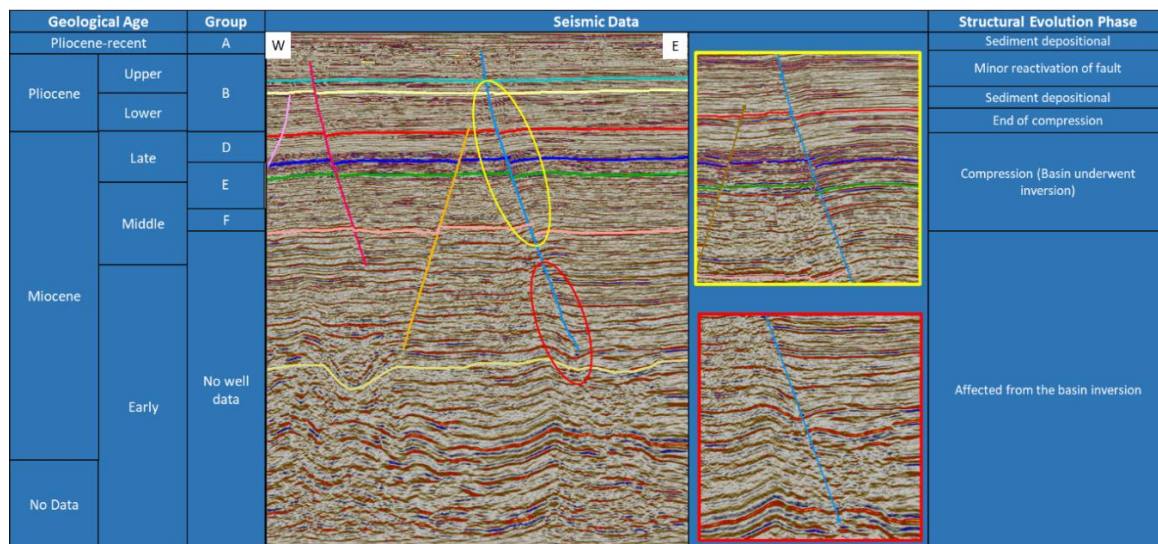


Figure 10. Explained the structural evolution phase from seismic data interpretation and well data

4. Conclusion

Based on the analysis of seismic attribute volume, structure and 3D structural modelling (Figure 11), this detailed study has interpreted the evolution of the North-western part of Malay basin. This study area was interpreted as a faulted anticline structure which segmented by two major faults. The faults geometry is mainly controlled by a normal fault. A major E-W normal fault separates this area into North and South segments. This fault terminates against the main N-S extensional normal fault. Others than two major fault E-W and N-S faults, some faults are reactivated faults that evolved from sedimentation load or accumulation after the compression which activated mild extensional tectonic activity.

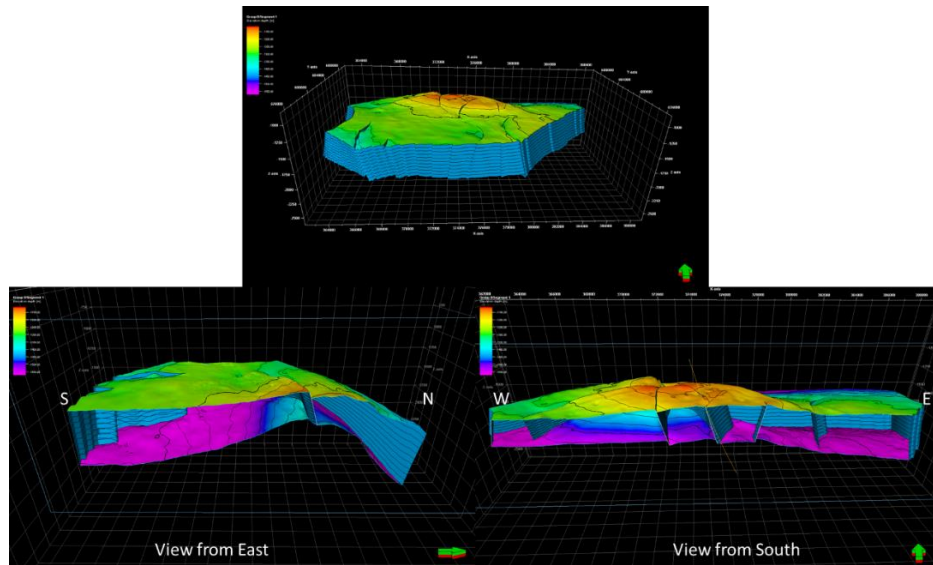


Figure 11. Showing the 3D structural model of study area and focus of lithology Group E

List of symbols

N	North	W	West
S	South	LMax	Length Maximum
E	East	DMax	Displacement Maximum

Acknowledgements

I would like to express my gratitude to Dr Deva Prasad Ghosh and Dr Rosita who helping, coaching and companionship with my master research. A big thank for PETRONAS for providing the necessary information and data to carry out this research work. Next, I would like to thank the members of CSI for their contribution and collaboration in completing some tasks in this project.

References

- [1] Madon M, Abolins P, Hoesni MJ, and Ahmad M. The Petroleum Geology and Resources of Malaysia, Petroliaam Nasional Berhad (PETRONAS), 1999; Chapter 8; p. 174–217.
- [2] Kong LK. Structural analysis of the Malay Basin. Bull. Geol. Soc. Malaysia. 1996; 40:156-176.
- [3] Mansor Y, Rahman AHA, Menier D, and Pubellier M. Structural evolution of Malay Basin, its link to Sunda Block tectonics. Mar. Pet. Geol. 2014; 58: 736–748.
- [4] Tjia HD. The Petroleum Geology and Resources of Malaysia, Petroliaam Nasional Berhad (PETRONAS), 1999; Chapter 7; p. 141–169.
- [5] Tjia HD. Origin and tectonic development of Malay-Penyu-West Natuna basins, Bull. Geol.Soc. Malaysia. 1998; 42: 147–160.
- [6] Maga D, Jong J, Madon M, and Kessler FL. Fluid inclusions in quartz: Implications for hydrocarbon charge, migration and reservoir diagenetic history of the penyu basin and tenggol arch, offshore peninsular Malaysia. Bull. Geol. Soc. Malaysia. 2015; 61: 59–73.
- [7] Zoback MD. Reservoir Geomechanics, 1st ed.; Cambridge University Press, 2007; Part 1; p. 3-24.
- [8] Madon M, Yang JS, Abolins P, Abu Hassan R, Yakzan AM, and Zainal SB. Petroleum systems of the Northern Malay Basin. Bull. Geol. Soc. Malaysia. 2006; 49: 125-134.
- [9] Tjia HD. Inversion tectonics in the Malay Basin: evidence and timing of events. Bull. Geol. Soc. Malaysia. 1994; 56: 119–126.
- [10] Madon M. The kinematics of extension and inversion in the Malay Basin, offshore Peninsular Malaysia. Bull. Geol. Soc. Malaysia. 1997; 41: 127–138.
- [11] Pubellier M and Morley CK. The basins of Sundaland (SE Asia): Evolution and boundary conditions. Mar. Pet. Geol. 2013; 58: 1–24.

To whom correspondence should be addressed: Siti Sorhana Syazwani Mokhtar, Department of Geoscience, Universiti Teknologi PETRONAS, 32610 Seri Iskandar, Malaysia, E-mail: siti_18003357@utp.edu.my